Waste Disposal & Sustainable Energy (2023) 5:1–11
https://doi.org/10.1007/s42768-022-00120-4

ARTICLE

Nitrite sensor using activated biochar synthesised by microwave-assisted pyrolysis

Scarlett Allende[1] · Yang Liu[2] · Muhammad Adeel Zafar[1] · Mohan V. Jacob[1]

Received: 25 August 2022 / Revised: 23 October 2022 / Accepted: 6 November 2022 / Published online: 17 January 2023

Abstract

Developing applications for the by-products obtained from waste processing is vital for resource recovery. The synthesis of $ZnCl_2$-activated biochar with high electrocatalytic activity was carried out by the microwave-assisted pyrolysis of pineapple peel and subsequent chemical activation process. Activated biochar is employed in the electrochemical sensing of nitrite by drop casting in a glassy carbon electrode (GCE). The activated biochar exhibited a stacked carbon sheet, 254 $m^2\ g^{-1}$ Brunauer, Emmett and Teller (BET) surface area, 0.076 $cm^3\ g^{-1}$ pore volume, 189.53 $m^2\ g^{-1}$ micropore area and oxygen-containing functional groups. The electrochemical impedance spectroscopy of the modified GCE showed a reduced charge transfer resistance of 61%. This is crucial to determine the electrochemical properties of biochar. The sensor showed a significant current response and an excellent limit of detection of 0.97 µmol L^{-1}. The modified-activated biochar electrochemical sensor demonstrated high selectivity, reproducibility (RSD=2.4%), and stability (RSD=2.6%).

Graphical abstract

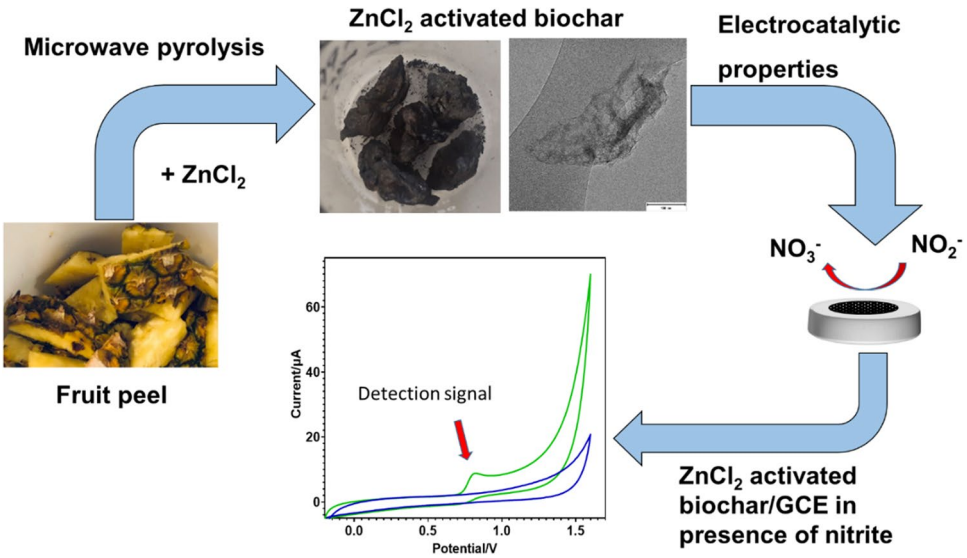

Keywords Microwave-assisted pyrolysis · Biochar · Nitrite · Electrochemical sensor

✉ Mohan V. Jacob
Mohan.Jacob@jcu.edu.au

[1] Electronics Material Lab, College of Science and Engineering, James Cook University, Townsville, QLD 4811, Australia

[2] College of Science and Engineering, James Cook University, Townsville, QLD 4811, Australia

Introduction

The agricultural industry generates around 23.7 million tonnes of food per day globally [1], but one-third of the solid food produced annually is wasted [2]. Food wastes cause 8%

of global greenhouse gas emissions [3]. Apart from food, agricultural waste residues also have negative impacts on the environment and economy [4–6]. The agricultural residues are classified into two types: agricultural wastes (husk, seed, bagasse, leaves) and industrial residues (orange peel, coconut oil cake, cassava peel, soybean oil cake, etc.) [7]. The depletion and excessive use of natural sources have caused a greater interest in renewable materials generated from waste in the agricultural sector [8–10]. The efficient and rapid conversion of agro-industrial waste into valuable products is highly desirable for reducing greenhouse gases related to waste accumulation [8, 11].

The conversion of solid agri-food waste into value-added products, i.e., biochar, bio-oil and biogas, can transform an unvalued material into versatile opportunities and applications [1, 12, 13]. Microwave-assisted pyrolysis of agri-food waste could efficiently convert by-products into a valued carbon material due to its electromagnetic heating allowing instantaneous volumetric heating and uniform distribution in the energetic coupling [14–16]. The synthesis of modified biochar from natural waste using microwave pyrolysis is an attractive alternative to producing ecological sensing materials [17–19]. The fabrication of biochar-modified electrodes can be done in two ways, i.e., drop casting on glassy carbon electrodes (GCE) or by making the carbon paste of the biochar [18]. The application of biochar-modified electrodes allows the determination of different analytes associated with the food, agriculture, and medical industries [17, 18]. The satisfactory detection capacity depends on the electrochemical and morphological properties of the biochar achieved during its activation process [18, 20, 21].

The activation of biochar can be attained by two main mechanisms: physical and chemical activation methods. The physical modification consists of thermal treatment that produces more pore volume and a larger surface area [11, 22]. For example, biomass activated by microwave pyrolysis can improve the surface area and surface functional groups. The improved composition of biochar can promote electron transfer and ion insertion rate [8, 18, 20]. The chemical activation implicates exposing the biomass or biochar (before or after pyrolysis) to chemical agents, such as nitric, sulfonic, phosphoric, and sulphuric acids. The activation through metal salt agents, i.e., $ZnCl_2$ produces dehydration of the carbon during the pyrolysis process, generating carbonyl and carboxylate functional groups [8, 20].

For the biochar activation, the literature shows different biomass feedstock, thermal and chemical methods. However, the relationship between the intrinsic properties of activated biochar and electrochemical sensor performance has not been completely studied. The purpose of this paper is to synthesise electrocatalytic biochar using pineapple peel as a biomass feedstock and microwave-assisted pyrolysis as a thermochemical treatment. The experimental parameters of the microwave-assisted pyrolysis process were essential for developing a biochar material with sensing properties and analytical performance. The physicochemical and electrochemical characterisation of activated biochar indicated high biochar Brunauer, Emmett and Teller (BET) surface area, micropore structure, increased pore volume, notable charge transferability, good selectivity and high carbon stability.

Experimental

Biochar synthesis using microwave-assisted pyrolysis

The breakdown of biomass using microwave pyrolysis involves electromagnetic volumetric heating in the absence of air to produce biochar, bio-oil, and biogas [15, 23, 24]. The microwave heating method transfers the energy through the interaction of the molecules inside the biomass rather than by heat transfer from external sources (dielectric heating) [16, 25]. The advantages of microwave-assisted pyrolysis are high heating efficiency, rapid reaction time, and control over heating [23, 26, 27]. Unlike conventional pyrolysis, microwave irradiation generates biochar with a higher fixed carbon content, significant thermal decomposition of the lignin network, better carbon stability and higher surface area and pore volume [28–30]. The heating rate (~ 132 °C min^{-1}) of microwave pyrolysis is beneficial for the activation of biochar because it promotes the formation of microporous structures, develops oxygen functional groups on the surface, and gives rise to catalytic properties [28, 31–33]. Therefore, the thermochemical treatment of pineapple peel biomass and modified biochar was carried out using microwave-assisted pyrolysis.

Figure 1 shows the microwave pyrolysis scheme used, which comprises N_2 flow (5 L min^{-1}) that maintains an inert atmosphere during the experiments; a custom-made chamber where the biomass is placed; a reflected power controller; a 3 kW microwave generator; power controller; various condensers, whose functionality is collect liquid and gas by-products; and a vacuum pump. The synthesis process of $ZnCl_2$-activated biochar comprises three stages. The first phase is biochar production using microwave-assisted pyrolysis. For this, pineapple peel was first washed with ethanol and distilled water. The cleaned biomass was dried in an oven at 110 °C for 24 h to reduce its moisture content to 10%. Then, the biomass was pyrolysed at 3 kW for 30 min. The produced biochar was soaked in $ZnCl_2$ for 24 h for chemical activation. Afterwards, the biochar was dried overnight in an oven at 110 °C. The third phase comprised the second pyrolysis (calcination process) of activated biochar at 1.5 kW for 20 min. After the activated biochar was cooled to room temperature, it was washed with 1 mol L^{-1}

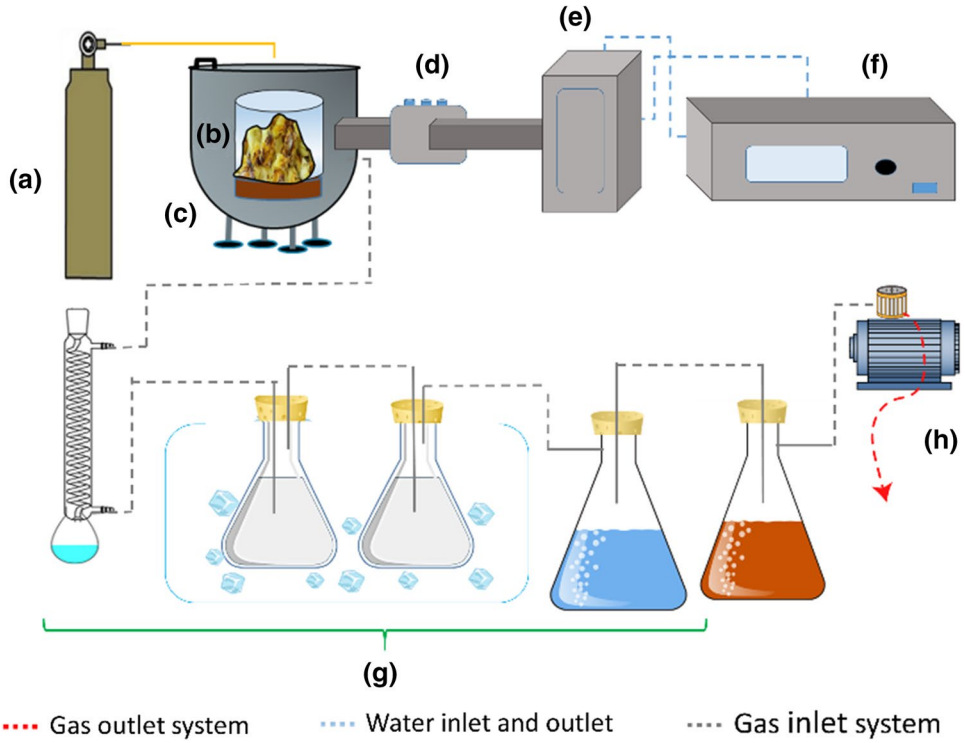

Fig. 1 Microwave pyrolysis system used in the $ZnCl_2$-activated biochar synthesis. The system components are (**a**) nitrogen gas cylinder; (**b**) quartz beaker containing biomass of pineapple peel; (**c**) custom-made pyrolysis chamber; (**d**) tuner; (**e**) microwave generator; (**f**) microwave power controller; (**g**) condensers; (**h**) vacuum pump

HCl and distilled water. Finally, the modified biochar was dried at 110 °C overnight.

Electrode preparation for electrochemical study

The powder-activated biochar was dispersed in ethanol and subjected to ultrasonic cleaning for 30 min. The electrochemical study was carried out by a three-electrode system. A GCE, Ag/AgCl electrode and platinum wire were used as working, reference and counter electrodes, respectively. The GCE surface was polished with 0.3 µmol L^{-1} and 0.5 µmol L^{-1} alumina slurry to remove impurities before coating. Subsequently, it was cleaned with ultra-sonification for 10 min in ethanol and deionised water. The GCE was dried at room temperature. Last, the GCE was coated with 2 µL of 1.5 mg mL^{-1} $ZnCl_2$-activated biochar using the drop-casting technique.

Reagents and instruments

Sodium nitrite ($NaNO_2$), zinc chloride ($ZnCl_2$, 1 mol L^{-1}), and hydrochloric acid (1 mol L^{-1}) were purchased from Sigma Aldrich. The phosphate-buffered saline (PBS, pH 7.0) solution was prepared using dibasic-Na_2HPO_4 and monobasic-NaH_2PO_4. Biomass feedstock applied in the production of modified biochar was pineapple peel which was obtained as food waste. The electrochemical experiments were carried out on PalmSens4 potentiostat (PalmSens, Houten, Netherlands). The characterisation techniques of the material involve the following: surface area obtained from micromeritics 3-flex surface and porosity analyser; transmission electron microscopy (TEM) imaging acquired from JEOL 2100 200 kV Transmission Electron Microscope (Joel, Peabody, MA, USA); X-ray photoelectron spectroscopy (XPS) using a Kratos Axis Supra (AXIS Supra$^+$, Manchester, UK); Raman spectrum was collected using a Renishaw In-Via Micro-Raman spectrometer (inVia Qontor, Keyborough, Australia); thermogravimetric analysis (TGA) was achieved using Netzsch STA 449F3 Jupiter Simultaneous Thermal Analyser (Netzsch, Wittelsbacherstrasse, Germany).

Result and discussion

Characterisation of $ZnCl_2$-activated biochar

Table 1 shows the FlashSMART CHNSO elemental analysis of non-activated and activated biochar. The ultimate analysis of raw biomass showed oxygen as the main component (50%). The progressive thermochemical treatment causes partial chemical oxygen removal and increased carbon content [28, 30]. The reduced O/C and H/C ratios indicate that during microwave pyrolysis decarboxylation reaction ensued, leading to a strong bond formation (carbon bonding) and decreased oxygen concentration [28, 31, 32]. Unlike raw biomass, the carbon content increased in $ZnCl_2$-activated biochar by 18%, and the oxygen

Table 1 Elemental analysis of raw biomass, activated and non-activated biochar

Sample	N%	C%	H%	O%	H/C	O/C
Pineapple peel	1.4	43.37	5.83	49.4	0.13	1.13
Non-activated biochar	1.02	69.25	1.37	7.27	0.02	0.11
$ZnCl_2$-activated biochar	1.52	51.39	1.32	12.31	0.026	0.24

concentration decreased by 75%. However, after the chemical activation, the H/C ratio in $ZnCl_2$-activated biochar was slightly higher (32%) than that in non-activated biochar, and the O/C value increased up to 0.24. According to the literature, the reduction of carbon content is related to the formation of amorphous microporous structures of aromatic sheets, which occurs after the chemical activation and second pyrolysis process [34]. The increased O/C ratio indicates the formation of oxygen functional groups during the thermochemical modification process of biochar [35–37]. Specifically, the biochar activation process with $ZnCl_2$ promotes the formation of carbonyl and hydroxyl

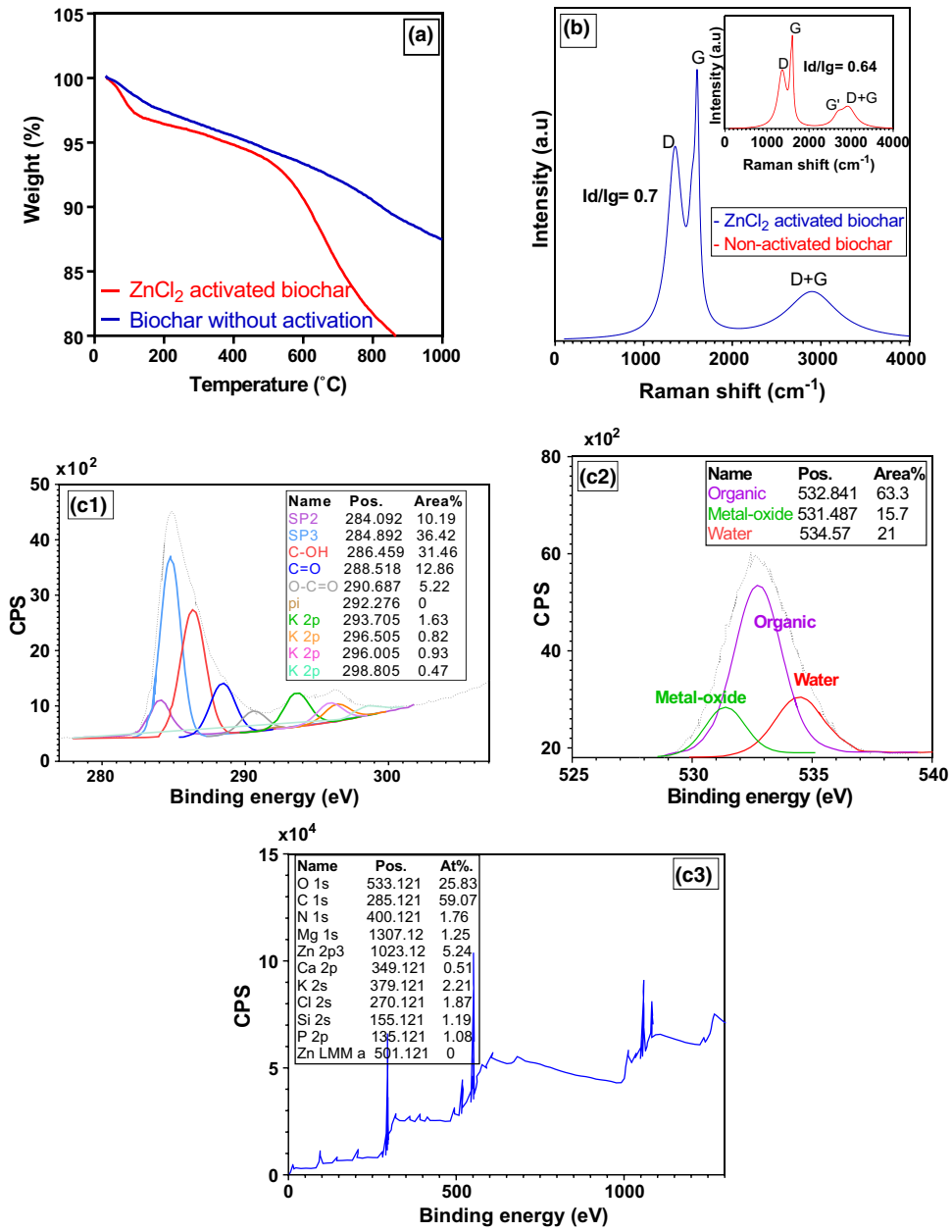

Fig. 2 (**a**) TGA curves of non-activated biochar generated at 3 kW for 30 min and activated biochar produced after chemical activation and second pyrolysis process at 1.5 kW for 20 min, (**b**) Raman spectra, and (**c1**)–(**c3**) XPS of $ZnCl_2$-activated biochar

groups (XPS data, Fig. 2c1) [35, 38]. The presence of oxygen-containing functional groups in biochar improves the physical adsorption and total capacitance of modified electrodes [39, 40].

The microwave-assisted biomass activation (thermal pretreatment) is attached to operational conditions, i.e., microwave power and reaction time. High input power leads to micropore formation, and extended exposure to microwave irradiation involves a higher surface area and pore volume [28, 35, 41]. Between 400 °C and 900 °C was reached at a 1.5–3 kW power range for 20–30 min. The high heating rate made microwave pyrolysis an appropriate thermal decomposition method for quick biomass breakdown (cracking of organic matter) [35, 41]. During the microwave pyrolysis process at 3 kW, biochar rapidly releases H_2 and CH_4, and produces carbonyl and carboxylate groups, which develop a higher surface area and micropores [18, 20, 38]. These physicochemical characteristics are essential for catalytic activity [20, 42, 43].

$ZnCl_2$ impregnation acts as an activating agent, causing the generation of deep cavities on the biochar. The BET surface area and pore volume of the activated biochar increased to 254.91 $m^2\ g^{-1}$ and 0.076 $cm^3\ g^{-1}$, respectively. After the activation, the micropores also increased up to 189.53 $m^2\ g^{-1}$. Micropore formation contributes to the electrocatalytic performance of modified electrodes by improving the adsorption of the analyte, facilitating the electrical conductivity and enhancing the sensor response [20, 44]. Table 2 shows the specific surface area comparison between unmodified and modified biochar.

Figure 3a, b shows scanning electron microscope (SEM) images of the biochar produced from the impregnation of $ZnCl_2$ and the calcination process. The activation process had a notable impact on the surface structure of the biochar, causing a high concentration of pore formation with uniform distribution. Specifically, the penetration of $ZnCl_2$ into the biochar pores generates an expansion of pores through all the biochar surfaces, explaining the increased pore volume [45]. Also, instead of a solid structure, the formation of thin sheets was observed in $ZnCl_2$-activated biochar. Figure 3c1, c2 shows a high sheet carbon structure, semi-organised carbon layers, and stacked sheets. No crystalline rods or crystalline patches were observed.

Table 2 BET data of activated and non-activated biochar

Analysis	Non-activated biochar	$ZnCl_2$-activated biochar
Surface area		
BET surface area ($m^2\ g^{-1}$)	88.51	254.91
t-Plot micropore area ($m^2\ g^{-1}$)	39.50	189.53
t-Plot external surface area ($m^2\ g^{-1}$)	49.01	65.38
BJH adsorption cumulative surface area of pores (1.7 nm and 300 nm diameter)	25.45	27.10
Pore volume		
t-Plot micropore volume ($cm^3\ g^{-1}$)	0.02	0.076
Total pore volume calculated < 1.0228 nm ($cm^3\ g^{-1}$)	0.03	0.09

BET Brunauer, Emmett and Teller

TGA of activated and non-activated biochar is shown in Fig. 2a. The results show that between 32 °C and 150 °C, there is slightly more weight loss in $ZnCl_2$-activated biochar (5%) than in the non-activated biochar (3%). The main reason is the moisture loss and adsorption of organic components at an early stage. Between 500 °C and 650 °C, the activated biochar suffered a higher weight loss (10%), which can be attributed to the thermal decomposition of pineapple peel compounds (holocellulose and lignin structures) and inorganic impurities [46–48]. At temperatures of 700 °C and 850 °C, the activated biochar was less affected by the volatilisation of the agent ($ZnCl_2$) inside pores, increasing the thermal decomposition resistance [49, 50]. Thus, the TGA curve indicates that non-activated biochar is more thermally stable than $ZnCl_2$-activated biochar.

Figure 2b shows the Raman spectrum of the biochar, showing a D-band at 1355 cm^{-1} and a G-band at 1620 cm^{-1} [17, 51]. Specifically, the D-band is due to the condensed existence of benzene rings in the amorphous carbon structure, and the G-band comprises the aromatic ring in biochar [52]. Moreover, the D + G peak (observed at 2899 cm^{-1}) describes the sp2 graphitic structure [53]. The results were similar to the Raman spectra of graphite oxide reported in [54]. An increase in the I_D/I_G factor was observed after the biochar activation, whose I_D/I_G value in $ZnCl_2$-activated biochar was 9.4% higher than that in non-activated biochar. A higher peak intensity ratio represents a large disordered (amorphous carbon atoms) and reduced graphite structure of biochar [34, 55, 56]. The high pyrolysis temperature of 3–1.5 kW could cause a change in the biochar structure. Figure 2c1–c3 shows the XPS spectrum of the activated biochar. Along with carbon, nitrogen, and oxygen were the principal components. Some metals were detected, i.e., Zn, Fe and Mg. High oxidation of carbon in the form of C–OH, O–C=O and C=O was observed. The C=O, O–C=O and C–OH structures are associated with carbonyl, ester and hydroxyl groups, respectively [57]. The carbonyl functional groups are formed due to the extraction of the H group from aromatic rings, whose reactions occur during the microwave pyrolysis and activation process [38]. XPS results revealed that using microwave pyrolysis as thermal treatment (high temperature) and $ZnCl_2$ as a chemical activator generates biochar with high carbon content and oxygen functionalities [39, 40, 58]. These characteristics are relevant to

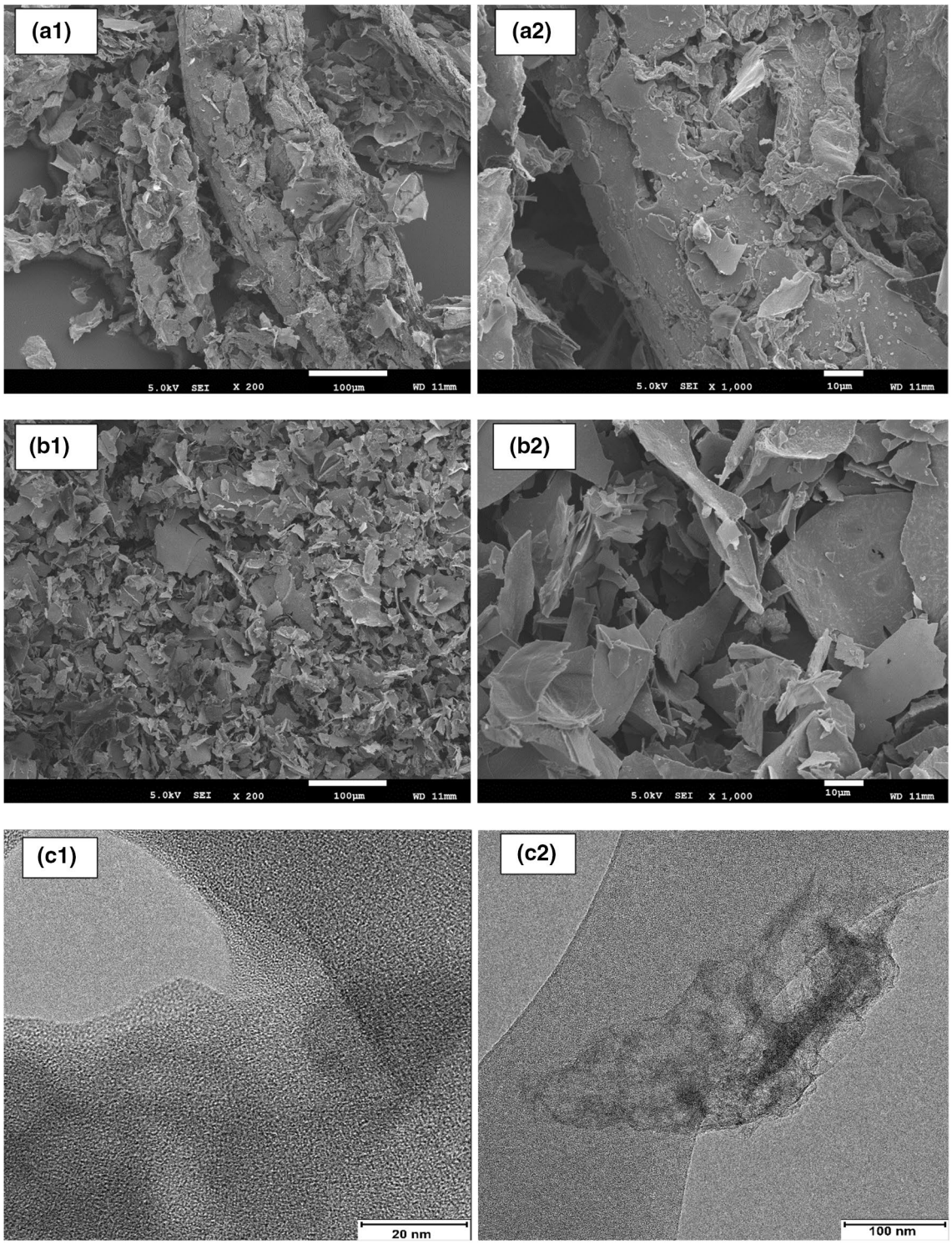

Fig. 3 Scanning electron microscope (SEM) images of (**a1**), (**a2**) non-activated biochar obtained at 3 kW for 30 min; (**b1**), (**b2**) SEM of $ZnCl_2$-activated biochar after chemical activation and calcination process at 1.5 kW for 20 min; (**c1**), (**c2**) high-resolution transmission electron microscopy (HRTEM) of $ZnCl_2$-activated biochar

determine the electrochemical performance of activated biochar. The discussion is developed in "Electrochemical characterisation".

Electrochemical characterisation

The electrochemical behaviour of bare GCE and $ZnCl_2$ activated biochar/GCE was investigated by electrochemical impedance spectroscopy (EIS) and cyclic voltammetry (CV) techniques. The EIS method evaluates the charge transfer resistance (kinetics) at the surface of the $ZnCl_2$-activated biochar/GCE. The impendence curve comprises a semi-circular area at higher frequencies and a linear portion, which is related to the electron transfer limited process and the diffusion process at lower frequencies, respectively [17, 42, 59, 60]. The diameter symbolises the electron transfer resistance (R_{ct}), whose value depends on the dielectric properties of the modified electrode interface [17, 42].

Figure 4 shows the Nyquist plots obtained through EIS. The measurement parameters in the experimental procedure consist of a 10^5 to 0.1 Hz frequency range and a 5 mV potential amplitude in 0.1 mol L^{-1} KCl containing 5.0 mmol L^{-1} $K_3[(Fe(CN)_6)]$. The EIS curves show that the diameter of bare GCE (R_{ct}=280 Ω) is higher than that of the $ZnCl_2$ activated biochar/GCE (R_{ct}=110 Ω). Increased micro porous structure (189.53 m^2 g^{-1}) and surface area (254.91 m^2 g^{-1}) of activated biochar promoted the adsorption properties, contributing to the accessibility and diffusion of the electrolyte into the porous structure. These can improve the charge electron transfer and sensor response. Moreover, higher conductivity is achieved due to the binding affinity between oxygen-containing functional groups on the surface of activated biochar and the analyte [39, 44]. These results confirm that $ZnCl_2$-activated biochar enhanced the electron transfer kinetic properties of the modified electrode.

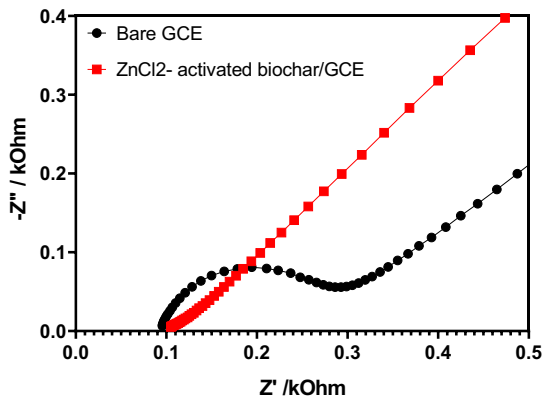

Fig. 4 Electrochemical impedance spectra of bare GCE (glassy carbon electrodes) and $ZnCl_2$-activated biochar/GCE in 0.1 mol L^{-1} KCl containing 5 mmol L^{-1} $K_3[(Fe(CN)_6)]$ at 5 mV s^{-1}

The electrocatalytic property of the modified electrode towards nitrite oxidation was studied in 0.1 mol L^{-1} PBS containing 0.7 mmol L^{-1} nitrite, as represented in Fig. 5. There was no oxidation response in the blank solution in either of the two electrodes (curves a and b). Bare GCE showed a minor oxidation peak with a peak current of 8 µA in nitrite solution at 1 V (curve c). By comparison, $ZnCl_2$-activated biochar/GCE presented a higher peak current of 19 µA (curve d) than non-modified GCE. A high surface area and increased micropore volume of $ZnCl_2$-activated biochar on the GCE improved the contact area between the biochar and the analyte, contributing to the charge propagation along the porous structure. Thus, using $ZnCl_2$-activated biochar as a modification material for the GCE enhanced the oxidation peak current and electrocatalytic activity.

Electrochemical detection of nitrite on $ZnCl_2$ activated biochar/GCE

The current responses of $ZnCl_2$-activated biochar/GCE in chronoamperometry for nitrite detection are shown in Fig. 6. The technical setting used was 0.8 V potential, whose value was optimal for the response to noise ratio. The concentration range applied was from 10 µmol L^{-1} to 2850 µmol L^{-1}, 250 µmol L^{-1} per interval. The current response of modified GCE increased proportionally to the nitrite addition ranging. The calibration curve between concentration and the current signal shows a direct relationship. The linear regression function is represented as $I(\mu A) = 0.0627\left(\mu mol\, L^{-1}\right) - 1.392, R^2 = 0.9939$. The limit of detection (LOD) achieved was 0.97 µmol L^{-1}. Table 3 shows a comparison of linear ranges and LOD in previous studies. The performance exhibited by $ZnCl_2$-activated

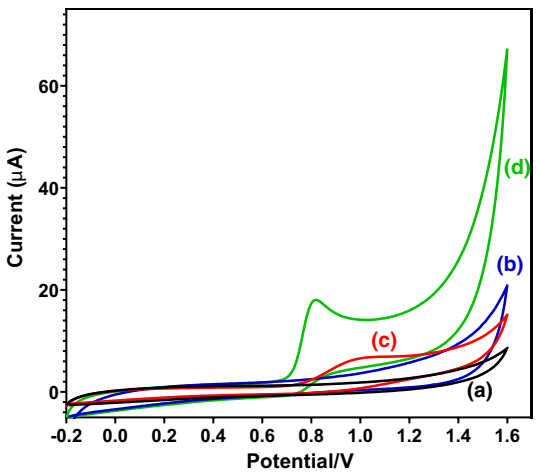

Fig. 5 Cyclic voltammetry response of bare GCE and $ZnCl_2$-activated biochar/GCE in the absence (**a**, **b**) and presence of 0.7 mmol L^{-1} nitrite (**c**, **d**) in 0.1 mol L^{-1} phosphate buffer solution (pH 7.0) at a 50 mV s^{-1} scan rate

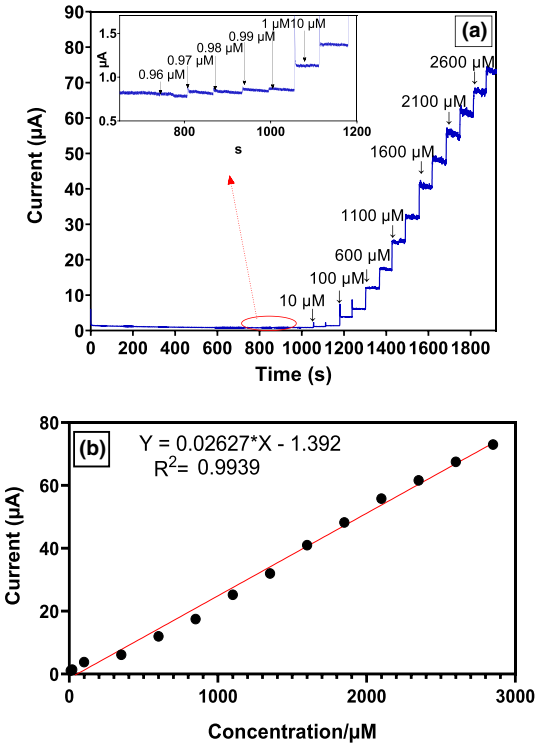

Fig. 6 (**a**) Chronoamperometry response of $ZnCl_2$-activated biochar/GCE at successive addition of $NaNO_2$ in 0.1 mol L^{-1} PBS (pH 7.0). (**b**) Calibration curve for nitrite concentration against peak currents. *PBS* phosphate-buffered saline, *μM* μmol L^{-1}

Table 3 Comparison of the analytical performance of nitrite sensor with various modified electrodes

Electrode	Linear range (μmol L^{-1})	LOD (μmol L^{-1})	Reference
ABC-800/GCE	4.9–1184	2.7	[21]
GCE/CeO2NPs	0.02–1200	0.21	[42]
Cu^{2+} $^{-}$Cu/biochar	1–300	0.63	[17]
Au/CuNi-based hollow nano-architecture (CNHN)	0.05–1150	0.017	[60]
Cu/multi-walled carbon nanotubes (MWCNTs)/GCE	5–1260	1.8	[61]
reduced graphene oxide- multi-walled carbon nanotubes-platinum nanoparticles/myoglobin (RGO-MWCNT-Pt)/Mb/GCE	1–1200	0.93	[62]
$ZnCl_2$-activated biochar/GCE	100–1400	0.97	This work

LOD limit of detection

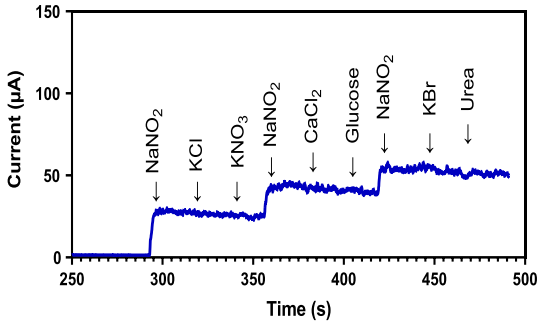

Fig. 7 Anti-interference property of $ZnCl_2$-activated biochar/GCE towards the detection of nitrite in the presence of electroactive species KCl, KNO_3, $CaCl_2$, glucose, KBr and urea

biochar/GCE was better or comparable to the electrochemical sensors reported in the literature.

Several studies indicate the addition of metal (copper, silver and gold) as the principal source for synthesising electrocatalytic active materials [17, 21, 42, 61, 62]. Some papers reported the use of conventional pyrolysis heating, hydrothermal and exfoliation procedure. Due to the sophisticated synthesis methods, the $ZnCl_2$-activated biochar/GCE showed lower charge transfer resistance (less than 150 Ω) compared to that of some materials registered in [17, 60, 61]. The CV response of the modified GCEs was similar to that of our activated biochar, showing a significant oxidation current peak. These electrocatalytic properties make $ZnCl_2$-activated biochar an excellent material for nitrite detection. Several studies indicate the addition of metal (copper, silver and gold) as the principal source for synthesizing electrocatalytic active materials [17, 21, 42, 61, 62]. Some papers reported the use of conventional pyrolysis heating, hydrothermal and exfoliation procedures. Due to the sophisticated synthesis methods, the $ZnCl_2$-activated biochar/GCE showed lower charge transfer resistance (less than 150 Ω) than some materials registered in [17, 60, 61]. The CV response of modified GCEs was similar to that of our activated biochar, showing a beneficial oxidation current peak. These electrocatalytic properties make $ZnCl_2$-activated biochar an excellent material for nitrite detection.

Selectivity, stability, and reproducibility of $ZnCl_2$-activated biochar/GCE

The chronoamperometry response of $ZnCl_2$-activated biochar/GCE and the effect of interfering substances on the peak current response of $NaNO_2$ are shown in Fig. 7. The anti-interference property of the modified GCE was studied considering 1 mmol L^{-1} nitrite, followed by the separate addition of 1 mmol L^{-1} of six potential interfering components into the stirred PBS at 0.8 V working potential. The results revealed that the presence of KCl, KNO_3, $CaCl_2$,

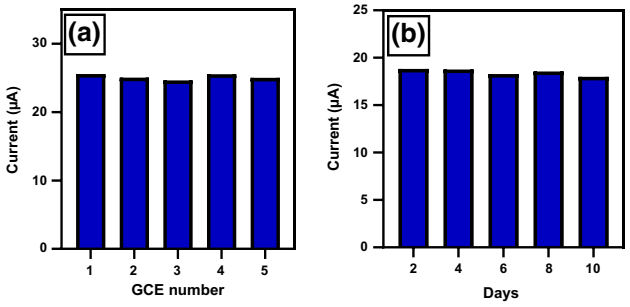

Fig. 8 (**a**) Reproducibility analysis of five $ZnCl_2$-activated biochar/GCE in the presence of 0.3 mmol L^{-1} nitrite in 0.1 mol L^{-1} PBS; (**b**) stability results of modified GCE in 0.25 mmol L^{-1} of nitrite in 0.1 mol L^{-1} PBS (pH 7.0)

glucose, KBr and urea did not influence the determination of $NaNO_2$. A notable response was observed for nitrite injections, but a weak current signal was observed for electroactive species additions. Therefore, it can be rightly said that $ZnCl_2$-activated biochar/GCE demonstrates excellent selectivity.

The reproducibility and stability of the modified glassy carbon were studied by differential pulse voltammetry (DPV). This technique was appropriate to determine the nitrate response, unlike chronoamperometry, DPV provided clarity to observe the oxidation current peaks using low nitrate concentrations. The reproducibility and stability of the $ZnCl_2$-activated biochar/GCE electrode are shown in Fig. 8a and b, respectively. Five GCEs were modified using $ZnCl_2$-activated biochar to evaluate their reproducibility for 0.3 mmol L^{-1} nitrite in 0.1 mol L^{-1} PBS (pH 7.0) solution. The results show that the modified GCEs have significant reproducibility behaviour, with a relative standard deviation (RSD) value of 2.4%. Then, the stability was evaluated for the electrochemical nitrite sensor every two days until the completion of ten days of storage at room temperature. The test was achieved in a 0.1 mol L^{-1} PBS (pH 7.0) solution containing 0.25 mmol L^{-1} nitrite. The DPV measurements for stability analysis demonstrate consistency in oxidation current response of up to 10 days, observing an excellent RSD of 2.6%.

Conclusions

This work synthesised the biochar through microwave pyrolysis and studied its electrochemical performance. Microwave-assisted pyrolysis had a significant role in the development of higher fixed carbon content, improved thermal decomposition of the lignin network, better carbon stability, and higher surface area and pore volume. The biochar was activated by soaking in $ZnCl_2$. The activated biochar showed amorphous microporous structures of aromatic sheets, oxygen-containing functional groups on the biochar surface, strong carbon bonding, and a relatively higher I_D/I_G peak intensity ratio (owing to the amorphous form of carbon). These properties facilitated the adsorption of the analyte and enhanced the electrocatalytic activity and hence the sensor response. Modified GCE presented a higher peak current (19 μA) compared to that of bare GCE (9 μA) and reduced the charge transfer resistance value (110 Ω). The electrochemical behaviour of $ZnCl_2$-activated biochar/GCE for nitrite detection revealed comparable LOD (0.97 μmol L^{-1}), and high selectivity, leading to the promising potential for real applications.

Supplementary Information The online version contains supplementary material available at https://doi.org/10.1007/s42768-022-00120-4.

Acknowledgements Scarlett Allende acknowledges the financial support of the Cooperative Research Centre for Developing Northern Australia and the support of its investment partners: the Western Australian, Northern Territory and Queensland Governments. We also acknowledge the financial and in-kind support of the project participants.

Data availability Data is available on the request to the corresponding author.

Declaration

Conflict of interest The authors declare no competing interests.

References

1. Duque-Acevedo, M., Belmonte-Ureña, L.J., Cortés-García, F.J., et al. 2020. Agricultural waste: Review of the evolution, approaches and perspectives on alternative uses. *Global Ecology and Conservation* 22: e00902. https://doi.org/10.1016/j.gecco.2020.e00902.
2. Adejumo, I.O., and Adebiyi., O.A. 2020. Agricultural solid wastes: Causes, effects, and effective management. *Strategies of Sustainable Solid Waste Management*. https://doi.org/10.5772/intechopen.93601.
3. Department of the Environment and Energy. 2017. National food waste strategy: Halving Australia's food waste by 2030. The Australian Government, National Food Waste Strategy, [Online]. https://www.dcceew.gov.au/sites/default/files/documents/national-food-waste-strategy.pdf

4. Awasthi, M.K., Lukitawesa, L., Duan, Y., et al. 2022. Bacterial dynamics during the anaerobic digestion of toxic citrus fruit waste and semi-continues volatile fatty acids production in membrane bioreactors. *Fuel* 319: 123812. https://doi.org/10.1016/j.fuel.2022.123812.
5. Wainaina, S. Awasthi, M.K., Sarsaiya, S., et al. 2020. Resource recovery and circular economy from organic solid waste using aerobic and anaerobic digestion technologies. *Bioresource Technology* 301: 122778. https://doi.org/10.1016/j.biortech.2020.122778.
6. Wu, H.-Y., Chen, S.S., and Liao, W. 2020. Assessment of agricultural waste-derived activated carbon in multiple applications. *Environmental Research* 191: 110176. https://doi.org/10.1016/j.envres.2020.110176.
7. Sadh, P.K., Duhan, S., and Duhan, J.S. 2018. Agro-industrial wastes and their utilization using solid state fermentation: A review. *Bioresources and Bioprocessing* 5 (1): 1. https://doi.org/10.1186/s40643-017-0187-z.
8. Kalinke, C., de Oliveira, P.R., Bonacin, J.A., et al. 2021. State-of-the-art and perspectives in the use of biochar for electrochemical and electroanalytical applications. *Green Chemistry* 23 (15): 5272–5301. https://doi.org/10.1039/d1gc00843a.
9. Liu, T., Miao, P., Shi, Y., et al. 2022. Recent advances, current issues and future prospects of bioenergy production: A review. *Science of The Total Environment* 810: 152181. https://doi.org/10.1016/j.scitotenv.2021.152181.
10. Cai, Z., Ye, F., Xie, Z., et al. 2021. The choice of cooperation mode in the bioenergy supply chain with random biomass feedstock yield. *Journal of Cleaner Production* 311: 127587. https://doi.org/10.1016/j.jclepro.2021.127587.
11. Wu, P., Wang, Z., Wang, H., et al. 2020. Visualizing the emerging trends of biochar research and applications in 2019: A scientometric analysis and review. *Biochar* 2 (2): 135–150. https://doi.org/10.1007/s42773-020-00055-1.
12. Dhanya, B.S., Mishra, A., Chandel, A.K., et al. 2020. Development of sustainable approaches for converting the organic waste to bioenergy. *Science of the Total Environment* 723: 138109. https://doi.org/10.1016/j.scitotenv.2020.138109.
13. SarangiSingh, P.K. T.A., Singh, N.J., et al. 2022. Sustainable utilization of pineapple wastes for production of bioenergy, biochemicals and value-added products: A review. *Bioresource Technology* 351: 127085. https://doi.org/10.1016/j.biortech.2022.127085.
14. GeYek, S. P.N.Y., Cheng, Y.W., et al. 2021. Progress in microwave pyrolysis conversion of agricultural waste to value-added biofuels: A batch to continuous approach. *Renewable and Sustainable Energy Reviews* 135: 110148. https://doi.org/10.1016/j.rser.2020.110148.
15. Hadiya, V., Popatac, K., Vyas, S., et al. 2022. Biochar production with amelioration of microwave-assisted pyrolysis: Current scenario, drawbacks and perspectives. *Bioresource Technology* 355: 127303. https://doi.org/10.1016/j.biortech.2022.127303.
16. Ethaib, S., Omar, R., Kamal, S.M.M., et al. 2020. Microwave-assisted pyrolysis of biomass waste: A mini review. *Processes* 8 (9): 1190. https://doi.org/10.3390/pr8091190.
17. Cao, L., Kang, Z.-W., Ding, Q., et al. 2020. Rapid pyrolysis of Cu^{2+}-polluted eggshell membrane into a functional Cu^{2+}-Cu^{+}/biochar for ultrasensitive electrochemical detection of nitrite in water. *Science of The Total Environment* 723: 138008. https://doi.org/10.1016/j.scitotenv.2020.138008.
18. Spanu, D., Binda, G., Dossi, C., et al. 2020. Biochar as an alternative sustainable platform for sensing applications: A review. *Microchemical Journal* 159: 105506. https://doi.org/10.1016/j.microc.2020.105506.
19. Zhang, D., Li, Y., Sun, A., et al. 2019. Enhanced nitrobenzene reduction by modified biochar supported sulfidated nano zerovalent iron: Comparison of surface modification methods. *Science of The Total Environment* 694: 133701. https://doi.org/10.1016/j.scitotenv.2019.133701.
20. Cheng, B.H., Zeng, R.J., and Jiang, H. 2017. Recent developments of post-modification of biochar for electrochemical energy storage. *Bioresource Technology* 246: 224–233. https://doi.org/10.1016/j.biortech.2017.07.060.
21. Sudha, V., Senthil Kumar, S.M., and Thangamuthu, R. 2019. Hierarchical porous carbon derived from waste amla for the simultaneous electrochemical sensing of multiple biomolecules. *Colloids and Surfaces. B, Biointerfaces* 177: 529–540. https://doi.org/10.1016/j.colsurfb.2019.01.029.
22. Zhang, Q., Xu, S., Cao, Y., et al. 2022. Sustainable production of gluconic acid and glucuronic acid via microwave-assisted glucose oxidation over low-cost Cu-biochar catalysts. *Green Chemistry* 24 (17): 6657–6670. https://doi.org/10.1039/D2GC02568J.
23. Li, X., Peng, B., Liu, Q., et al. 2022. Microwave pyrolysis coupled with conventional pre-pyrolysis of the stalk for syngas and biochar. *Bioresource Technology* 348: 126745. https://doi.org/10.1016/j.biortech.2022.126745.
24. Wang, W., Wang, M., Huang, J., et al. 2020. High efficiency pyrolysis of used cigarette filters for ester-rich bio-oil through microwave-assisted heating. *Journal of Cleaner Production* 257: 120596. https://doi.org/10.1016/j.jclepro.2020.120596.
25. Yu, H., Qu, J., Liu, Y., et al. 2022. Co-pyrolysis of biomass and polyvinyl chloride under microwave irradiation: Distribution of chlorine. *Science of The Total Environment* 806: 150903. https://doi.org/10.1016/j.scitotenv.2021.150903.
26. Toscano Miranda, N., Lopes Motta, I., Maciel Filho, R., et al. 2021. Sugarcane bagasse pyrolysis: A review of operating conditions and products properties. *Renewable and Sustainable Energy Reviews* 149: 111394. https://doi.org/10.1016/j.rser.2021.111394.
27. Zhang, Y., Zhou, C., Deng, Z., et al. 2022. Influence of corn straw on distribution and migration of nitrogen and heavy metals during microwave-assisted pyrolysis of municipal sewage sludge. *Science of The Total Environment* 815: 152303. https://doi.org/10.1016/j.scitotenv.2021.152303.
28. Mari Selvam, S., and Paramasivan, B. 2022. Microwave assisted carbonization and activation of biochar for energy-environment nexus: A review. *Chemosphere* 286: 131631. https://doi.org/10.1016/j.chemosphere.2021.131631.
29. Tang, Y.-H., Liu, S.-H., and Tsang, D.C.W. 2020. Microwave-assisted production of CO_2-activated biochar from sugarcane bagasse for electrochemical desalination. *Journal of Hazardous Materials* 383: 121192. https://doi.org/10.1016/j.jhazmat.2019.121192.
30. Hidalgo, P., Navia, R., Hunter, R., et al. 2019. Synthesis of carbon nanotubes using biochar as precursor material under microwave irradiation. *Journal of Environmental Management* 244: 83–91. https://doi.org/10.1016/j.jenvman.2019.03.082.
31. Yek, P.N.Y., Peng, W., Wong, C.C., et al. 2020. Engineered biochar via microwave CO_2 and steam pyrolysis to treat carcinogenic Congo red dye. *Journal of Hazardous Materials* 395: 122636. https://doi.org/10.1016/j.jhazmat.2020.122636.
32. Lam, S.S., Yek, P.N.Y., Ok, Y.S., et al. 2020. Engineering pyrolysis biochar via single-step microwave steam activation for hazardous landfill leachate treatment. *Journal of Hazardous Materials* 390: 121649. https://doi.org/10.1016/j.jhazmat.2019.121649.
33. Sun, Y., Zhang, Q., Clark, J.H., et al. 2022. Tailoring wood waste biochar as a reusable microwave absorbent for pollutant removal: Structure-property-performance relationship and iron-carbon interaction. *Bioresource Technology* 362: 127838. https://doi.org/10.1016/j.biortech.2022.127838.
34. Lay, M., Rusli, A., Abdullah, M.K., et al. 2020. Converting dead leaf biomass into activated carbon as a potential replacement

for carbon black filler in rubber composites. *Composites Part B: Engineering* 201: 108366. https://doi.org/10.1016/j.compositesb.2020.108366.
35. Godwin, P.M., Pan, Y., Xiao, H., et al. 2019. Progress in preparation and application of modified biochar for improving heavy metal ion removal from wastewater. *Journal of Bioresources and Bioproducts* 4 (1): 31–42. https://doi.org/10.21967/jbb.v4i1.180.
36. Hassan, M., Liu, Y., Naidu, R., et al. 2020. Influences of feedstock sources and pyrolysis temperature on the properties of biochar and functionality as adsorbents: A meta-analysis. *Science of the Total Environment* 744: 140714. https://doi.org/10.1016/j.scitotenv.2020.140714.
37. Yang, Q.-L., Qin, Z., Liu, H.-M., et al. 2021. Performance of sesame straw cellulose, hemicellulose, and lignin biochars as adsorbents in removing benzo(a)pyrene from edible oil. *Food Science and Technology*. https://doi.org/10.1590/fst.49021.
38. Sajjadi, B., Zubatiuk, T., Leszczynska, D., et al. 2019. Chemical activation of biochar for energy and environmental applications: A comprehensive review. *Reviews in Chemical Engineering* 35 (7): 777–815. https://doi.org/10.1515/revce-2018-0003.
39. Dehkhoda, A.M., Ellis, N., and Gyenge, E. 2014. Electrosorption on activated biochar: Effect of thermo-chemical activation treatment on the electric double layer capacitance. *Journal of Applied Electrochemistry* 44 (1): 141–157. https://doi.org/10.1007/s10800-013-0616-4.
40. Liu, Q., Jiang, S., Su, X., et al. 2021. Role of the biochar modified with $ZnCl_2$ and $FeCl_3$ on the electrochemical degradation of nitrobenzene. *Chemosphere* 275: 129966. https://doi.org/10.1016/j.chemosphere.2021.129966.
41. Tomczyk, A., Sokołowska, Z., and Boguta, P. 2020. Biochar physicochemical properties: Pyrolysis temperature and feedstock kind effects. *Reviews in Environmental Science and Bio/Technology* 19 (1): 191–215. https://doi.org/10.1007/s11157-020-09523-3.
42. Tamizhdurai, P., Sakthinathan, S., Chen, S.M., et al. 2017. Environmentally friendly synthesis of CeO_2 nanoparticles for the catalytic oxidation of benzyl alcohol to benzaldehyde and selective detection of nitrite. *Scientific Reports* 7: 46372. https://doi.org/10.1038/srep46372.
43. Yan, L., Liu, Y., Zhang, Y., et al. 2020. $ZnCl_2$ modified biochar derived from aerobic granular sludge for developed microporosity and enhanced adsorption to tetracycline. *Bioresource Technology* 297: 122381. https://doi.org/10.1016/j.biortech.2019.122381.
44. Casanova, A., Iniesta, J., and Gomis-Berenguer, A. 2022. Recent progress in the development of porous carbon-based electrodes for sensing applications. *The Analyst* 147 (5): 767–783. https://doi.org/10.1039/D1AN01978C.
45. Sun, K., Huang, Q., Chi, Y., et al. 2018. Effect of $ZnCl_2$-activated biochar on catalytic pyrolysis of mixed waste plastics for producing aromatic-enriched oil. *Waste Management* 81: 128–137. https://doi.org/10.1016/j.wasman.2018.09.054.
46. Sukruansuwan, V., and Napathorn, S.C. 2018. Use of agro-industrial residue from the canned pineapple industry for polyhydroxybutyrate production by Cupriavidus necator strain A-04. *Biotechnology for Biofuels* 11: 202. https://doi.org/10.1186/s13068-018-1207-8.
47. De Fatima Salgado, M., A.M. Abioye, M.M. Junoh, et al. 2018. Preparation of activated carbon from Babassu endocarpunder microwave radiation by physical activation. *IOP Conference Series: Earth and Environmental Science* 105: 012116. https://doi.org/10.1088/1755-1315/105/1/012116.
48. Raji, F., and Pakizeh., M. 2013. Study of Hg(II) species removal from aqueous solution using hybrid $ZnCl_2$-MCM-41 adsorbent. *Applied Surface Science* 282: 415–424. https://doi.org/10.1016/j.apsusc.2013.05.145.
49. Chatterjee, R., Sajjadi, B., Chen, W.-Y., et al. 2020. Effect of pyrolysis temperature on physicochemical properties and acoustic-based amination of biochar for efficient CO_2 adsorption. *Frontiers in Energy Research*. https://doi.org/10.3389/fenrg.2020.00085.
50. Nikkhah, H., Tavasoli, A., and Jafarian, S. 2020. Investigating the influence of acid washing pretreatment and Zn/activated biochar catalyst on thermal conversion of Cladophora glomerata to value-added bio-products. *Energy Conversion and Management* 225: 113392. https://doi.org/10.1016/j.enconman.2020.113392.
51. Alagarsamy, P. 2018. Amperometric determination of acetaminophen (paracetamol) using graphene oxide modified glassy carbon electrode. *International Journal of Electrochemical Science* 13: 7930–7938. https://doi.org/10.20964/2018.08.01.
52. Eshun, J., Wang, L., Ansah, E., et al. 2019. Characterization of the physicochemical and structural evolution of biomass particles during combined pyrolysis and CO_2 gasification. *Journal of the Energy Institute* 92 (1): 82–93. https://doi.org/10.1016/j.joei.2017.11.003.
53. Khan, A., Savi, P., Quaranta, S., et al. 2017. Low-cost carbon fillers to improve mechanical properties and conductivity of epoxy composites. *Polymers* 9 (12): 642.
54. Muzyka, R., S. Drewniak, T. Pustelny, et al. 2018. Characterization of graphite oxide and reduced graphene oxide obtained from different graphite precursors and oxidized by different methods using Raman Spectroscopy. *Materials* 11: 1050. https://doi.org/10.3390/ma11071050.
55. Yu, X., Han, X., Chang, C., et al. 2020. Corncob-derived activated carbon for roxarsone removal from aqueous solution: Isotherms, kinetics, and mechanism. *Environmental Science and Pollution Research* 27 (13): 15785–15797. https://doi.org/10.1007/s11356-020-07942-x.
56. Li, X., Song, Y., Bian, Y., et al. 2019. Effects of root exudates on the sorption of polycyclic aromatic hydrocarbons onto biochar. *Environmental Pollutants and Bioavailability* 31 (1): 156–165. https://doi.org/10.1080/26395940.2019.1593054.
57. Liu, C., Wang, W., Wu, R., et al. 2020. Preparation of acid- and alkali-modified biochar for removal of methylene blue pigment. *ACS Omega* 5 (48): 30906–30922. https://doi.org/10.1021/acsomega.0c03688.
58. Fan, X., Lu, Y., Xu, H., et al. 2011. Reversible redox reaction on the oxygen-containing functional groups of an electrochemically modified graphite electrode for the pseudo-capacitance. *Journal of Materials Chemistry* 21 (46): 18753–18760. https://doi.org/10.1039/C1JM13214H.
59. Haldorai, Y., Yeon, S.-H., Huh, Y.S., et al. 2017. Electrochemical determination of tryptophan using a glassy carbon electrode modified with flower-like structured nanocomposite consisting of reduced graphene oxide and SnO_2. *Sensors and Actuators B-Chemical* 239: 1221–1230. https://doi.org/10.1016/j.snb.2016.09.119.
60. Lei, P., Zhu, R., Wu, S., et al. 2020. Gold nanoparticles decorated bimetallic CuNi-based hollow nanoarchitecture for the enhancement of electrochemical sensing performance of nitrite. *Microchimica Acta* 187 (10): 572. https://doi.org/10.1007/s00604-020-04545-8.
61. Manoj, D., Saravanan, R., Santhanalakshmi, J., et al. 2018. Towards green synthesis of monodisperse Cu nanoparticles: An efficient and high sensitive electrochemical nitrite sensor. *Sensors Actuators B-Chemistry* 266: 873–882. https://doi.org/10.1016/j.snb.2018.03.141.
62. Mani, V., Dinesh, B., Chen, S.M., et al. 2014. Direct electrochemistry of myoglobin at reduced graphene oxide-multiwalled carbon nanotubes-platinum nanoparticles nanocomposite and biosensing towards hydrogen peroxide and nitrite. *Biosensors and Bioelectronics* 53 (420): 420–427. https://doi.org/10.1016/j.bios.2013.09.075.